Fluorescence Quenching in Electron-Donating Solvents. 2. Solvent Dependence and Product Dynamics

Morandeira, Ana; Fürstenberg, Alexandre; Vauthey, Eric

How to cite

MORANDEIRA, Ana, FÜRSTENBERG, Alexandre, VAUTHEY, Eric. Fluorescence Quenching in Electron-Donating Solvents. 2. Solvent Dependence and Product Dynamics. In: The journal of physical chemistry. A, 2004, vol. 108, n° 40, p. 8190–8200. doi: 10.1021/jp048048c

This publication URL: https://archive-ouverte.unige.ch/unige:3656
Publication DOI: 10.1021/jp048048c

Fluorescence Quenching in Electron-Donating Solvents. 2. Solvent Dependence and Product Dynamics

Ana Morandeira,‡ Alexandre Fürstenberg, and Eric Vauthey*

Department of Physical Chemistry of the University of Geneva, 30 quai Ernest-Ansermet, CH-1211 Genève 4, Switzerland

Received: May 6, 2004; In Final Form: July 5, 2004

The electron transfer quenching dynamics of excited perylene and cyanoperylene in various donating solvents has been investigated by using ultrafast fluorescence up-conversion and multiplex transient grating. The strongly nonexponential fluorescence decays have been analyzed by using the orientational model described in the first article of this series (*J. Phys. Chem. A* **2003**, *107*, 5375). It appears that the solvent dependence of the quenching dynamics is strongly connected to the number of surrounding donor molecules enabling ultrafast electron transfer. This number depends mainly on the driving force for electron transfer, on steric interactions, and on the occurrence of dipole−dipole interactions with the acceptor. The quenching product is an exciplex with a strong charge-transfer character. The complicated wavelength dependence of the fluorescence dynamics in the exciplex region, as well as the spectral dynamics observed in the transient grating data, is attributed to dipolar solvation, which leads to an increase of the charge-transfer character of the exciplex. The strong donor dependence of the exciplex lifetime is very similar to that reported earlier for the charge recombination time of geminate ion pairs in acetonitrile, and can be rationalized in terms of different intramolecular reorganization energies and electronic coupling constants.

Introduction

Over the past few years, a rather large number of investigations on the dynamics of electron transfer (ET) quenching in reactive solvents have been carried out.[1−12] The primary goal of these studies was the determination of the intrinsic rate constant of ET between an excited molecule and a quencher in liquid solutions. Indeed, since the pioneering work of Weller and co-workers,[13] it has been well-known that bimolecular ET quenching in an inert solvent is, in many cases, diffusion-limited and therefore the quenching rate constant does not deliver much information on the true ET dynamics. In principle, an adequate analysis of the transient effect observed in the decay of the excited-state population allows the intrinsic ET rate constant to be recovered.[14−19] However, such an analysis is rather complex and the result depends strongly on the model used to describe the ET rate constant and especially its distance dependence. Consequently, the study of the quenching dynamics in reacting solvents is an apparently more direct approach.

The most typical features of the excited-state population dynamics in a reacting solvent are its ultrafast and its strong nonexponential characters. In most cases, these excited state decays have been analyzed by using multiexponential functions. The faster decay component has been attributed to the reactant subpopulation with the most favorable mutual acceptor−donor geometry for ET and the corresponding decay constant was generally interpreted as the rate constant of ET between the excited reactant and one donor molecule, i.e., $\tau_{fast}^{-1} = k_{ET}$. However, molecular dynamics calculations have evidenced that among the rather larger number of solvent molecules surrounding an excited molecule,[20] more than one can have an orientation favoring ultrafast ET.[11] In this case, the origin of the faster decay component of the excited state population should be reinterpreted as being due to the excited state subpopulation surrounded by the largest, statistically significant, number of solvent molecules with an ET active orientation. Therefore, the corresponding decay constant is in fact equal to the sum of the ET rate constants between the excited molecule and all the ET active solvent molecules, i.e., $\tau_{fast}^{-1} = \sum k_{ET,i}$. If the number of active solvent molecules is large, the ET rate constant deduced without taking this complication into account might be substantially overestimated.

In the first paper of this series (Paper 1),[1] we have presented an investigation of the quenching dynamics of perylene (Pe) and perylene derivatives in the first singlet excited state in *N*,*N*-dimethylaniline (DMA). A rather intriguing result of this study was that the quenching dynamics of the polar cyanoperylene (PeCN) is about 10 times faster than those measured with Pe and nonpolar derivatives, although the driving force for ET is almost the same for all acceptors. The nonexponential fluorescence decays of the excited acceptors were analyzed by using a new orientational model, where the solvent molecules surrounding the excited acceptors are sorted into three groups: donors with an optimal orientation for ultrafast ET, D_a, and donors for which ET is only effective after some rotational and translational diffusion, D_b and D_c, respectively. For the last two groups of molecules, ET is thus limited by rotational and translational diffusion, with rate constants k_R and k_T, respectively. The observed decay of the normalized fluorescence intensity, $I(t)$, is thus given by:

$$I(t) = \sum_{i=1}^{N} P_i \exp(-k_i t) \qquad (1)$$

‡ Present address: Department of Physical Chemistry of the University of Uppsala, 751 23 Uppsala, Sweden.

* Address correspondence to this author. E-mail: eric.vauthey@chiphy.unige.ch.

10.1021/jp048048c CCC: $27.50
Published on Web 09/08/2004

CHART 1: Electron-Donating Solvents

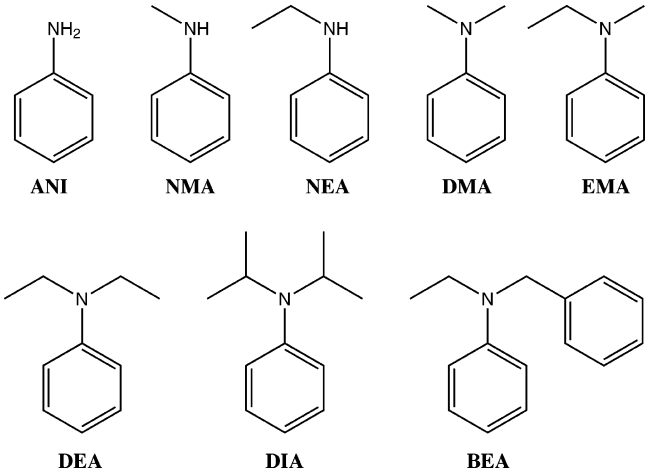

with N being the number of possible arrangements of solvent molecules around an acceptor, P_i the probability for the arrangement i to be realized, and k_i the rate constant for the decay of the acceptor surrounded with this arrangement of donors:

$$k_i = n_{ai}k_{ET} + n_{bi}k_R + n_{ci}k_T + k_{fl} \quad (2)$$

where n_{ai}, n_{bi}, and n_{ci} are the numbers of D_a, D_b, and D_c molecules in this arrangement, respectively, k_{ET} is the rate constant for ET between the acceptor and a D_a molecule, and k_{fl} is the rate constant of deactivation of the excited acceptor in a nonreacting solvent.

The probability P_i can be calculated with the following multinomial distribution:

$$P_i = \frac{n!}{n_{ai}!n_{bi}!n_{ci}!}(p_a)^{n_{ai}}(p_b)^{n_{bi}}(p_c)^{n_{ci}} \quad (3)$$

where p_a, p_b and p_c are the probabilities for a surrounding solvent molecule to be D_a, D_b and D_c, respectively.

Equation 1 was thus fitted to the experimental fluorescence decays with k_{ET}, p_a, and p_b as adjustable parameters and with $n = n_a + n_b + n_c$, k_R, and k_T as fixed parameters, calculated or taken from the literature. From this analysis, it appeared that the much faster quenching observed with PeCN could be explained by a larger average number of D_a molecules compared to the other acceptors, the ET rate constant k_{ET} remaining essentially the same, in agreement with the similar driving force. The larger number of D_a with PeCN was ascribed to the dipole−dipole interaction between PeCN and DMA, which favors mutual orientations with a large electronic coupling.

We present here an investigation on the influence of the nature of the electron-donating solvents on the quenching dynamics of Pe and PeCN. These solvents are shown in Chart 1. The quenching of coumarin dyes in some of these solvents has already been investigated by Shirota et al.[21] The average fluorescence lifetime was found to decrease by going from AN to *N*-monoalkylanilines and to *N*,*N*-dialkylanilines. Moreover, the size of the substituent was found to have no effect with *N*-monoalkylanilines. With *N*,*N*-dialkylanilines on the other hand, the average lifetime was found to increase with the size of the substituent. These differences were ascribed to orientational and distance effects, which influence the magnitude of the electronic coupling.

More recently, Castner et al. have investigated the quenching dynamics of coumarin 152 in methyl-substituted *N*,*N*-dimethylanilines.[11] The variation of the average fluorescence lifetime of the acceptor could be satisfactorily explained in terms of steric interactions, the excited-state lifetime increasing with decreasing distance between the methyl and the amino groups.

The dynamics of the product formed upon ET quenching in donor solvents has been studied in a few cases only. The radical pair resulting from the quenching of oxazine in DMA was found to decay by charge recombination within a few picoseconds.[6,22] A similar result was reported for rhodamine 6G in DMA and DEA.[12] On the other hand, the product of the quenching of 9-cyanoanthracene in DMA was reported to be an exciplex, whose dynamics could be measured by fluorescence.[9,10] In all these cases, the dynamics of product formation was found to be the same as the decay dynamics of the excited acceptor population.

In this paper, we also present an investigation of the dynamics of the quenching product monitored by both fluorescence up-conversion and the transient grating techniques. The combination of these two methods allows a clear picture of the fine details of product formation to be obtained.

Experimental Section

Time-Resolved Measurements. The fluorescence up-conversion and the time-correlated single-photon counting (TCSPC) setups have already been described in Paper 1.

A detailed description of the multiplex transient grating (TG) setup can be found in ref 23. Excitation was performed at 400 nm with the frequency-doubled output of a standard 1 kHz amplified Ti:Sapphire system (Spitfire, Spectra-Physics). The pulse duration was around 100 fs. All TG spectra were corrected for the chirp of the probe pulses.

Samples. Perylene (Pe) was recrystallized in benzene before use. 3-Cyanoperylene (PeCN) was synthesized according to the litterature[24] and was purified by column chromatography. Aniline (ANI, Fluka), *N*-methylaniline (NMA, Fluka), *N*-ethylaniline (NEA, Aldrich), *N*,*N*-dimethylaniline (DMA, Fluka), *N*,*N*-diethylaniline (DEA, Acros), *N*-ethyl-*N*-methylaniline (EMA, Aldrich), *N*,*N*-diisopropylaniline (DIA, Aldrich), and *N*-benzyl-*N*-ethylaniline (BEA, Aldrich) were distilled at reduced pressure under inert atmosphere.[25] Chlorobenzene (CB, Fluka, puriss.) was used as received. The viscosity of the electron-donating solvents was measured with a capillary viscosimeter (Schott Geräte).

For up-conversion measurements, the samples were placed in a spinning cell of 0.4 mm path length. The concentration of the samples was adjusted to obtain an absorbance at 400 nm of 0.1−0.15 on 0.4 mm. This corresponds to a concentration of $2-3 \times 10^{-4}$ M. For TCSPC measurements, a 1 cm thick quartz cell was used and the absorbance at 395 nm was around 0.1. For TG measurements, the sample solutions were placed in a 1 mm thick cell. The absorbance of the solution at 400 nm was around 0.2 on 1 mm. During the measurements, the solutions were continuously stirred by N_2 bubbling.

All the measurements were carried out at 20 °C. All the solutions were purged with Ar for 15−20 min before the fluorescence measurements. The presence of oxygen had no influence on the fluorescence dynamics of Pe and PeCN in the donating solvents. On the other hand, the long exciplex fluorescence lifetimes measured by TCSPC may be somewhat affected by imperfect deoxygenation of the solutions.

The fluorescence data analysis has been described in detail in Paper 1.

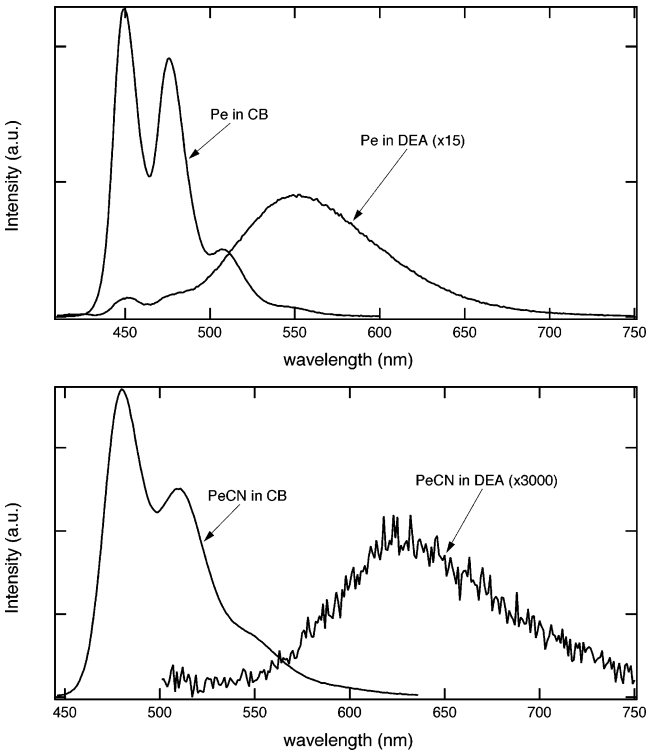

Figure 1. Steady-state fluorescence spectra of Pe (top) and PeCN (bottom) in CB and in DEA.

Results

Steady-State Measurements. The UV−vis absorption spectra of the acceptors Pe and PeCN in the electron-donating solvents are very similar to those measured in inert solvents. No new band that could be ascribed to the formation of a ground-state complex could be detected. In the aniline derivatives investigated here, the absorption spectra of Pe and PeCN do not exhibit any significant solvent dependence.

The fluorescence spectra of Pe and PeCN in CB and in DEA are shown in Figure 1. CB is a nonreactive solvent with both a static dielectric constant ($\epsilon_s = 5.6$) and a refractive index ($n = 1.524$) similar to those of the donating solvents.[26] In CB, the spectrum is due to the emission from the locally excited S_1 states of the acceptors. In DEA, these bands have almost totally disappeared and are replaced by a broad and structureless band that can be ascribed to exciplex emission. In inert solvents, such an exciplex emission of Pe with DEA and other aromatic amines is well documented.[27−29] Similar exciplex emissions can also be observed with Pe and PeCN in most reacting solvents used here, their maxima and quantum yields being listed in Table 1. This table shows that for a given solvent, the exciplex quantum yield is always larger with Pe. Similarly, the emission maxima of Pe exciplexes is always blue shifted compared to those with PeCN. This shift can be explained by the smaller S_1 energy and the better electron-acceptor property of PeCN (vide infra). For both acceptors, the exciplex fluorescence quantum yield increases in the order:

$$\text{ANI} < \text{NMA} < \text{NEA} < \text{DMA} \approx \text{EMA} < \text{DEA} < \text{DIA} < \text{BEA}$$

No exciplex emission could be observed with PeCN in ANI and NMA.

Time-Resolved Fluorescence Measurements. The fluorescence dynamics of Pe and PeCN in nonreactive solvents has already been discussed in detail in Paper 1. The early dynamics is wavelength dependent and is dominated by vibrational relaxation (VR).[30] This effect is the weakest between 460 and 490 nm for Pe and between 470 and 500 nm for PeCN. For this reason, the fluorescence decays of Pe and PeCN in donating solvents have been measured in these ranges. Moreover, the fluorescence time profiles during the first few picoseconds exhibit a weak but distinct oscillation associated to the excitation of a vibrational wave packet.[31] These oscillations are at 70 and 47 cm^{-1} for Pe and PeCN, respectively, and can be ascribed to low-frequency Raman modes of these molecules.[32,33]

In a longer time scale, the fluorescence intensity of Pe and PeCN in CB decays exponentially with lifetimes of 4.4 and 4.6 ns, respectively.

Figures 2 and 3 show the fluorescence decay of Pe and PeCN in several donating solvents. These decays were measured in the wavelength range specified above and are due to the local fluorescence of the acceptor. In this region, the fluorescence decays are not wavelength dependent, except for the system Pe/BEA (vide infra).

The decays of the local emission are strongly nonexponential for all acceptor/solvent systems except Pe/ANI. They can be reproduced by a stretched exponential function,[34] or by the sum of two or three exponential functions. The parameters obtained from a global multiexponential fit are listed in Tables 2 and 3 together with the average lifetime

$$\tau_{av} = I_0^{-1} \int_0^\infty I(t)\, dt \qquad (4)$$

with the time dependent fluorescence intensity, $I(t)$, and the maximum fluorescence intensity, I_0.

The fluorescence decay of the system Pe/BEA is wavelength dependent in the 460−490 nm range. This is due to a rather strong exciplex emission overlapping substantially with Pe local fluorescence. To avoid this contribution, the fluorescence decay of Pe was measured at 438 nm. At this wavelength, the fluorescence intensity exhibits an initial ultrafast decay that can be attributed to vibrational relaxation,[30] this component being

TABLE 1: Spectral Maxima, λ_{max}, Quantum Yields, Φ_E, and Lifetimes, τ_E, of the Exciplex Emission of Pe and PeCN in Electron-Donating Solvents

	Pe			PeCN		
solvent	λ_{max} (nm)	Φ_E	τ_E (ns)	λ_{max} (nm)	Φ_E	τ_E (ns)
ANI	550	3.2×10^{-4}	0.13 (0.14)[a]		$<5 \times 10^{-5}$	0.04[a]
NMA	578	3.5×10^{-4}	0.7		$<5 \times 10^{-5}$	0.12[a]
NEA	558	1.40×10^{-3}	1.8	630	6×10^{-5}	0.18 (0.15)[a]
DMA	570	0.040	37	650	1.1×10^{-4}	1.6
EMA	562	0.035	35	643	1.0×10^{-4}	1.4
DEA	551	0.067	60	630	3.0×10^{-4}	3.5
DIA	529	0.088	73	612	4.50×10^{-3}	24
BEA	527	0.208	63	604	0.016	29.5

[a] Decay time of the radical anion band measured by TG.

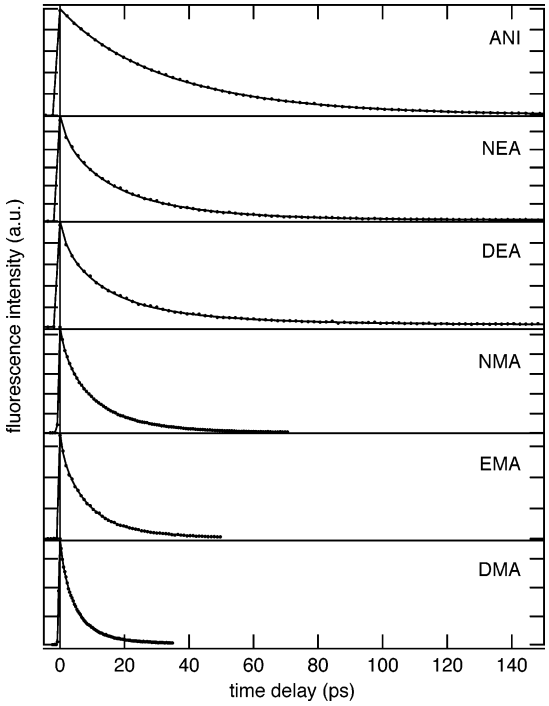

Figure 2. Time profiles of the local fluorescence of Pe in various electron-donating solvents and best multiexponential fits.

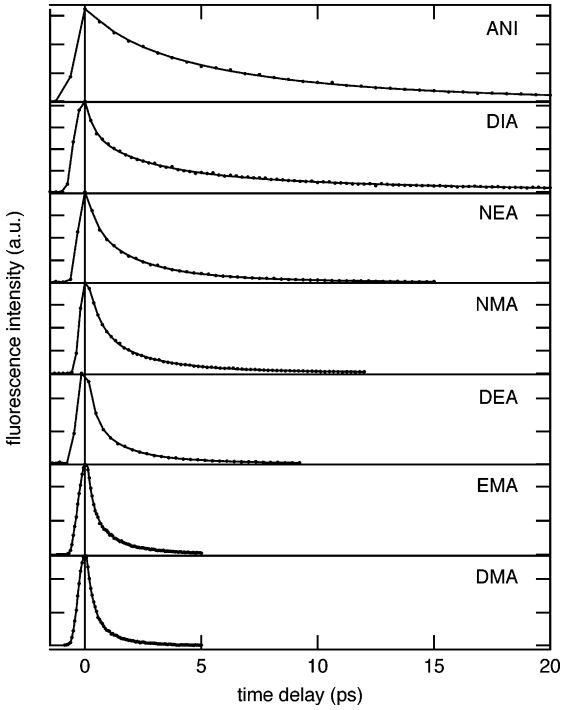

Figure 3. Time profiles of the local fluorescence of PeCN in various electron-donating solvents and best multiexponential fits.

present in both BEA and CB. The remaining part of the decay in BEA is very slow and exceeds the time window of the up-conversion setup. The fluorescence dynamics of Pe in BEA was therefore measured by TCSPC as well and the slower decay time was extracted from these data. This decay time was used as a fixed parameter in the analysis of the up-conversion data. The decay parameters related to the quenching of Pe in BEA are listed in Table 2.

The early fluorescence dynamics of the PeCN/DMA exciplex was measured in detail. The results are shown in Figure 4. The maximum fluorescence intensity at 670 nm is much smaller than

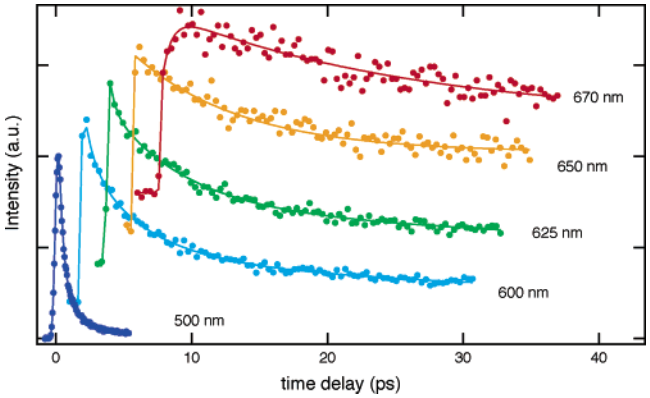

Figure 4. Wavelength dependence of the fluorescence dynamics of PeCN in DMA.

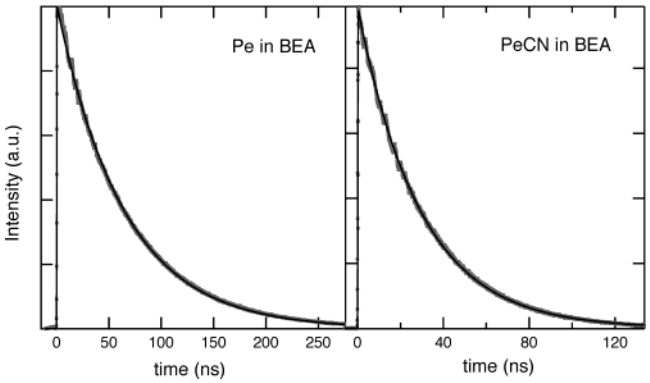

Figure 5. Exciplex fluorescence decays measured with Pe and PeCN in BEA and best exponential fits.

TABLE 2: Amplitudes, A_i, and Time Constants, τ_i, Obtained from a Triexponential Global Fit to the Fluorescence Time Profiles of Pe in Donating Solvents in the Wavelength Range 460−490 nm

solvent	A_1	τ_1 (ps)	A_2	τ_2 (ps)	A_3	τ_3 (ps)	τ_{av} (ps)
ANI	0.91	35.7	0.09	3.5			32.8
NMA	0.54	14.6	0.34	5.4	0.12	0.89	9.8
NEA	0.47	26.8	0.37	10.3	0.16	1.8	16.8
DMA	0.11	13.3	0.66	4.9	0.23	0.87	4.9
EMA	0.22	17.4	0.62	7.4	0.16	0.89	8.6
DEA	0.25	36.2	0.56	12.2	0.19	1.8	16.4
DIA	0.09	297	0.76	73.5	0.15	14.7	84.2
BEA[a]	0.73	850	0.27	90			640

[a] Fluorescence measured at 438 nm.

that at 500 nm. However, to facilitate comparison, the intensity of these profiles has been normalized. Each of these decays can be reasonably well reproduced with a biexponential function. The time constant of the fast component is of the order of 1 ps and its amplitude decreases with increasing wavelength, to become negative above 650 nm. The time constant of the slow component is not constant but increases with increasing wavelength. For example, it amounts to 7 and 18 ps at 600 and 670 nm, respectively. These decays cannot be fitted globally with less than six exponential functions. A qualitatively similar wavelength dependence was also found in the other solvents with both Pe and PeCN, but was not investigated in detail.

The slower exciplex fluorescence dynamics has been measured by TCSPC. Figure 5 shows the decay of the exciplex fluorescence of Pe and PeCN in BEA. All these exciplex fluorescence decays can be well reproduced with an exponential function with the lifetimes listed in Table 1. This table shows that for a given solvent, the exciplex lifetime is always shorter with PeCN than with Pe. Moreover, the solvent dependence of

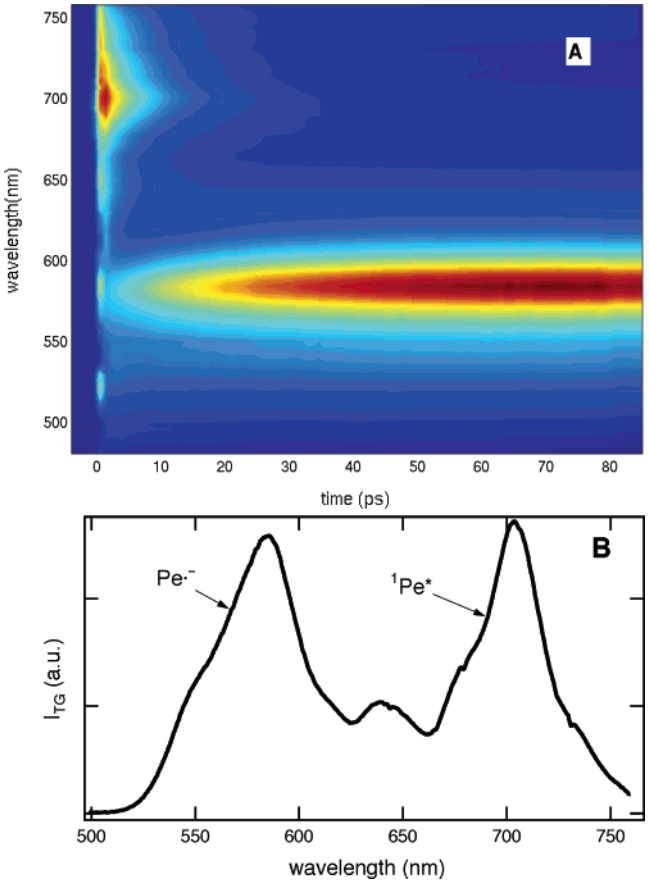

Figure 6. (A) Contour plot of the TG intensity measured with Pe in EMA after excitation at 400 nm and (B) cut along the wavelength axis at 8 ps.

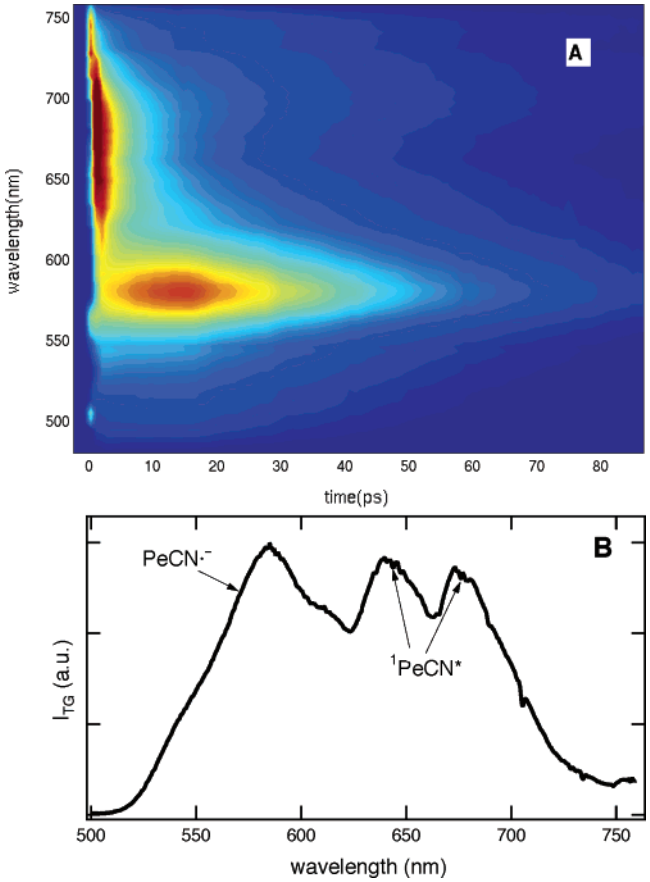

Figure 7. (A) Contour plot of the TG intensity measured with PeCN in ANI and (B) Cut along the wavelength axis at 6 ps.

the lifetime follows essentially the same trend as that found with the fluorescence quantum yield.

Multiplex TG Measurements. Multiplex TG measurements have been carried out in order to have more information on the nature of the primary ET quenching product. Figure 6A shows the contour plot of the TG intensity as a function of wavelength and time measured with Pe in EMA. As discussed in detail elsewhere,[35,36] the TG intensity is proportional to the square of the photoinduced changes of absorbance, ΔA, and refractive index, Δn:

$$I_{TG} = c_1 \Delta A^2 + c_2 \Delta n^2 \qquad (5)$$

where c_1 and c_2 are constants. In the time scale investigated here, Δn contains a contribution from the population changes, Δn_{pop}, which is Kramers−Kronig related to ΔA, and a contribution from the optical Kerr effect (OKE) arising from the solvent, Δn_{OKE}.[23] Most of the OKE is due to the electronic response and is only present during the temporal overlap of the pump and probe pulses. This contribution interferes with that from Δn_{pop} and, because of this, the TG intensity exhibits a spike at time zero. Depending on the sample, the intensity of this spike can be larger than that of the signal due to population changes. In this case, the analysis of the population dynamics near $\Delta t = 0$ is difficult. Figure 6B shows a cut in the data plotted in Figure 6A at $\Delta t = 8$ ps. As explained in detail in refs 37 and 38, such a TG spectrum is very similar to a transient absorption spectrum, the main difference being that the TG intensity is proportional to the square of the absorbance changes, and therefore the signal is insensitive to the sign of ΔA. The TG spectrum plotted in Figure 6B consists of two bands, one around 700 nm due to ^{1}Pe*,[39] and one at 570 nm that can be ascribed to the anion Pe$^{\bullet-}$.[40] Similar spectra have been obtained in the other donating solvents. Figure 7A shows a contour plot of the TG intensity measured with PeCN in ANI and a cut along the wavelength axis 6 ps after excitation is plotted in Figure 7B. The two peaks around 650 and 700 nm are also present in inert solvents and can be ascribed to ^{1}PeCN*, while the band at 570 is due to PeCN$^{\bullet-}$.[41]

The contour plots indicate that the decrease of the excited state band is accompanied by an increase of the radical anion band. However, these two kinetics are not identical. This is particularly evident in Figure 8A, which shows the time profile of the TG intensity at 700 and 570 nm measured with Pe in NMA. The decay at 700 nm can be well reproduced with a triexponential function with the same time constants and almost the same relative amplitudes as those obtained from the analysis of the fluorescence dynamics (see Table 2). However, the number of data points is considerably smaller than in the fluorescence measurements, with which a global fitting was performed. Therefore, a biexponential function with 1.4 and 12.3 ps can also be fitted to this TG time profile. The initial spike in the time profile of the TG intensity at 570 nm is due to the OKE. The rise of the TG intensity can be perfectly well reproduced with a single exponential function with a time constant of 19.2 ps. To see more clearly that the kinetics at 570 and 700 nm differ, a rise with the same time constants as those used to fit the 700 nm decay but with negative amplitudes is also plotted in Figure 8A. The difference between this rise and the experimental one is much larger than the noise of the data. Similar differences have also been observed in other donor solvents. The TG bands of ^{1}PeCN* and PeCN$^{\bullet-}$ are spectrally closer than with Pe, and therefore the dynamics of product

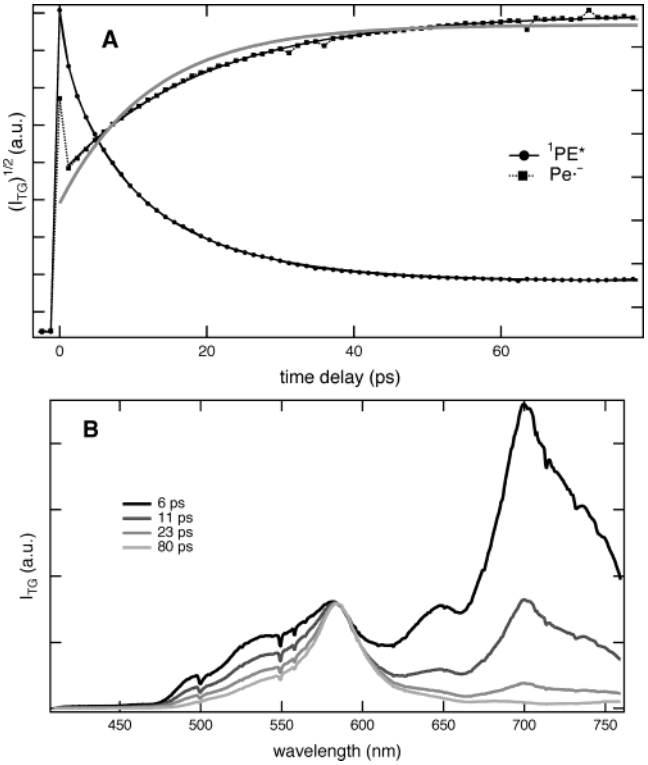

Figure 8. (A) Time profiles of the square root of the diffracted intensity at 700 and 570 nm measured with Pe in NMA. The continuous black lines are the best biexponential fits and the gray line is a biexponential rise with the same parameters as the decay at 700 nm but with negative amplitudes. (B) TG spectra measured with Pe in NMA at different time delays after excitation and normalized at the maximum of the radical anion band.

formation is much more difficult to extract. The interference with the OKE makes this even more problematic and therefore the rising dynamics of PeCN$^{\bullet-}$ was not investigated in detail.

A close look at the TG spectra collected at different time delays reveals that the shape of the Pe$^{\bullet-}$ band is time dependent. Figure 8B shows several TG spectra measured with Pe in NMA at different times after excitation. For a better comparison, their intensity has been normalized at the maximum of the Pe$^{\bullet-}$ band. This figure shows that this band becomes narrower with increasing time delay. The larger relative intensity on the blue side could be partially accounted for by the contribution of ^{1}Pe* population that has not been totally quenched at early time. However, the decay of the TG intensity on the blue side is considerably slower than that of ^{1}Pe*, indicating that a part of this spectral dynamics is unrelated to ^{1}Pe*. As discussed in more detail below, this spectral narrowing is probably connected to the delayed rise of the TG intensity at 570 nm.

After the initial rise, the intensity of both Pe$^{\bullet-}$ and PeCN$^{\bullet-}$ bands remains constant in most solvents in the time window of the TG measurements (0−120 ps). However, for Pe in ANI and PeCN in ANI, NMA, and NEA, the rise of the TG intensity is followed by a decay. Due to the limited time window of the experiment, only an approximate decay time of 140 ps can be determined for Pe$^{\bullet-}$ in ANI. For PeCN$^{\bullet-}$, these decay times are 40, 120, and about 150 ps in ANI, NMA, and NEA, respectively. Table 1 indicates that these decay times are essentially the same as the corresponding exciplex fluorescence lifetimes.

Discussion

Solvent Dependence of the Quenching Dynamics. The solvent dependence of the average fluorescence decay time of Pe and PeCN is somewhat similar to that observed with coumarins by Shirota et al.,[42] namely, the average time constant decreases in the order ANI, *N*-alkylanilines, and *N*,*N*-dialkylanilines. As also observed by these authors, τ_{av} increases with increasing size of the substituents on the *N*,*N*-dialkylanilines. Contrary to their study, the same trend is observed with *N*-alkylanilines. Another important feature is the systematically faster quenching dynamics observed with PeCN compared with Pe.

TABLE 3: Amplitudes, A_i, and Time Constants, τ_i, Obtained from a Triexponential Global Fit to the Fluorescence Time Profiles of PeCN in Donating Solvents in the Wavelength Range 470−500 nm

solvent	A_1	τ_1 (ps)	A_2	τ_2 (ps)	A_3	τ_3 (ps)	τ_{av} (ps)
ANI	0.46	10.0	0.40	3.6	0.14	0.94	6.2
NMA	0.04	7.4	0.31	2.0	0.65	0.49	1.2
NEA	0.14	5.0	0.40	1.7	0.46	0.35	1.5
DMA	0.01	2.5	0.13	0.97	0.86	0.30	0.42
EMA	0.04	2.4	0.15	0.84	0.81	0.24	0.42
DEA	0.08	3.8	0.31	1.2	0.61	0.30	0.88
DIA	0.22	11.1	0.36	2.3	0.42	0.36	3.5
BEA	0.27	67.2	0.32	10.4	0.41	1.3	22.2

TABLE 4: Van Der Waals Volumes, V_{vdw}, Orientational Diffusion Time Constants, τ_R, and Viscosity, η, at 20 °C of the Donating Solvents

solvent	V_{vdw} (Å^3)[a]	τ_R (ps)[b]	η (cP)
ANI	92.7	17.8	4.40[c]
NMA	110.2	16.2	2.35[c]
NEA	127.2	19.1	2.36[c]
DMA	127.7	24.6	1.41[c]
EMA	144.7		
DEA	161.7	36.9	2.16[d]
DIA	195.7		3.29[e]
BEA	214.1		26.4[e]

[a] Calculated according to ref 46. [b] From ref 21. [c] From ref 47. [d] From ref 48. [e] Measured here.

However, according to the orientational model described in detail in Paper 1, the average quenching time constant is not a direct measure of the ET dynamics, but depends on the number of solvent molecules in optimal geometry for ET and on the rotational and translational diffusion dynamics of the solvent molecules. This model, which was used successfully to discuss the quenching dynamics in DMA, will now be applied to analyze the fluorescence decay of Pe and PeCN in the other donating solvents.

An important factor in the application of this model is an adequate description of the rotational and translational diffusion of the donor molecules. Knowledge of k_R and k_T limits the number of adjustable parameters when fitting eq 1 to the data. Good estimates of k_R can be obtained from solvent dynamics measurements, such as microwave absorption, OKE, or dynamic Stokes shift. Microwave absorption and OKE measurements in ANI and DMA can be found in the literature.[43−45] On the other hand, the dynamic fluorescence Stokes shift measurements in ANI, MA, DMA, EA, and DEA have been reported by Shirota et al.[21] In general, two time constants are found in the picosecond time scale: one between 1 and 4 ps depending on the solvent, attributed to the inversion of the amino group, and a larger one, ascribed to the orientational diffusion. Therefore, this latter time constant will be used to account for the reorientation of the solvent molecules. The values of τ_R ($=1/k_R$) are listed in Table 4, together with the viscosity and the van der Waals volumes of the donor molecules.

As already pointed out by Yoshihara and co-workers,[45] the τ_R values of anilines cannot be simply discussed in terms of

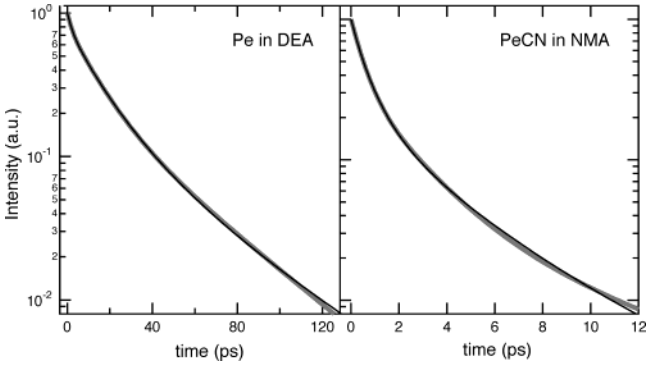

Figure 9. Comparison of the best fit of eq 1 with the triexponential function reproducing the fluorescence decay of (A) Pe in DEA and (B) PeCN in NMA.

the Stokes−Einstein−Debye (SED) equation (eq 4 in Paper 1). According to this expression, the τ_R value of ANI should be twice as large as that of DMA, while the experimentally measured value of ANI is about three times smaller than that of DMA. Similar smaller deviations from the SED equation can also be observed with NMA and NEA. On the other hand, the rotational time of DEA is longer than that of DMA as expected, but the difference is smaller than it should be according to the viscosity.

The apparent failure of the SED equation to interpret the rotational diffusion time of the anilines strongly compromises the estimation of the rotational time of EMA, DIA, and EBA. Nevertheless, a range of realistic values can be estimated for these solvents. For EMA, τ_R can be reasonably assumed to lie between those of DMA and DEA. Similarly for DIA and EBA, τ_R must be larger than that of DEA and smaller than the value calculated from the SED equation. Assuming the same shape factor and boundary condition as DEA, this equation predicts τ_R values of 68 and 600 ps for DIA and EBA, respectively.

In Paper 1, it was shown that the description of translational diffusion is not critical provided the number of D_a and D_b molecules is large. In this case, the quenching dynamics essentially does not involve translation. This was the case for Pe and PeCN in DMA, where k_T was calculated from the Stokes−Einstein equation,[46] and for which the experimental data could be very well reproduced by eq 1. This was, however, no longer the case with methylperylene (PeMe), whose quenching dynamics was substantially slower. The fluorescence decay of PeMe in DMA could only be reproduced with eq 1 when using a k_T value substantially smaller than that found from the Stokes−Einstein expression. However, this value was close to that calculated from the semiempirical expression of Spernol and Wirtz.[49] Because of this difficulty to estimate k_T, this parameter was not fixed during the data analysis. Moreover, the fit of eq 1 was performed with acceptor/donor systems with a relatively fast quenching dynamics, i.e., with $\tau_{av} < 20$ ps, for which the translational diffusion does not play too an important role.

As illustrated in Figure 9, the observed fluorescence time profiles could be very well reproduced with this orientational model. The resulting best-fit parameters are listed in Tables 5 and 6. With systems exhibiting ultrafast quenching, i.e., $\tau_{av} <$ 5 ps, the quality of the fit appeared to be almost independent of k_T, values ranging from 500 to 1500 ps giving essentially the same quality of the fit. Moreover, for PeCN in DEA and in EMA, the translational component of the quenching was found to be zero. For the analysis of the systems Pe/EMA, PeCN/EMA, and PeCN/DIA, τ_r was varied from 24.6 to 36.9 ps in EMA, and from 36.9 to 70 in DIA. The resulting τ_{ET} values were found to remain essentially constant.

TABLE 5: Parameters Obtained from the Fit of Eq 1 to the Fluorescence Decay of Pe in Various Electron-Donating Solvents[a]

solvent	n	τ_{ET} (ps)	τ_T (ps)	p_a	p_b	n_a	n_b
NMA	16	1.3	260	0.01	0.05	<1	<1
NEA	16	2.0	430	0.01	0.04	<1	<1
DMA	16	1.1	*b*	0.015	0.25	<1	4
EMA	15	1.0	300−500	0.01	0.15	<1	2−3
DEA	14	2.3	640	0.015	0.12	<1	1−2

[a] Number of molecules in the first solvent shell, n, ET time constant for optimal orientation, τ_{ET} ($=1/k_{ET}$), average number of donor molecules with optimal orientation, n_a, or requiring orientation, n_b, and related probabilities, p_a and p_b. [b] Could not be clearly determined.

TABLE 6: Parameters Obtained from the Fit of Eq 1 to the Fluorescence Decay of PeCN in Various Electron-Donating Solvents[a]

solvent	n	τ_{ET} (ps)	τ_T (ps)	p_a	p_b	n_a	n_b
ANI	17	1.93	210	0.017	0.077	<1	1−2
NMA	16	1.17	*b*	0.09	0.31	1−2	5
NEA	16	0.71	*b*	0.055	0.04	1	6−7
DMA	16	1.3	*b*	0.23	0.43	3−4	7
EMA	15	0.77	*b*	0.175	0.6−0.8	2−3	9−12
DEA	14	0.77	*b*	0.11	0.89	1−2	12−13
DIA	14	0.9−1.0	*b*	0.07	0.3−0.5	1	4−7

[a] Number of molecules in the first solvent shell, n, time constant of ET for optimal orientation, τ_{ET} ($=1/k_{ET}$), average number of donor molecules with optimal orientation, n_a, or requiring orientation, n_b, and related probabilities, p_a and p_b. [b] Could not be clearly determined.

The number of molecules in the first solvent shell, n, was estimated with the procedure described in detail in Paper 1. A variation of n of ±5 molecules was found to influence neither the resulting rate constants, i.e., k_{ET} and k_T, nor n_a, the average number of molecules in an optimal position for ET. However, when the dynamics is ultrafast and when n is smaller than 10, the model fails to reproduce the experimental data.

From Tables 5 and 6, it appears that in a given solvent, the ET time constant, τ_{ET}, is about the same for Pe and PeCN. The largest difference is found in DEA, where ET is about three times faster with PeCN. However, this difference is relatively small when considering that the average quenching time of PeCN is shorter by a factor of 19 compared with that of Pe. According to this orientational model, their distinct quenching dynamics are due to a different number of molecules in an optimal position for ET, n_a. As in Paper 1, we ascribe this difference to dipole−dipole interaction, which is only operative with PeCN and favors mutual acceptor−donor orientations with a high electronic coupling. Moreover, considering that diffusive solvation is essentially frozen in the ET time scale, dipole−dipole interaction could also lead to orientations of the solvent shell that favor ET, i.e., that minimize the solvent reorganization energy.

According to Tables 5 and 6, the ET time constants with Pe and PeCN do not vary significantly from one donating solvent to another. In principle, a variation of donating solvent should affect both the driving force for ET, ΔG_{ET}, and the solvent reorganization energy, λ_s.[50] The driving force, calculated with the Weller expression for the solvents of known oxidation potential,[51] and the solvent reorganization energies are listed in Table 7. This table shows that, although the range of ΔG_{ET} is narrow, the ET driving force increases from ANI to *N*-monoalkylanilines and to *N*,*N*-dialkylanilines. On the other hand, λ_s is around 0.5 eV in most solvents. The driving force for ET in EMA and the solvent reorganization energy can be expected to lie between those calculated for DMA and DEA. Finally for BEA and DIA, these ΔG_{ET} and λ_s values should not be largely different.

TABLE 7: Solvent and Electron-Transfer Parameters[a]

				ΔG_{ET} (eV)[c]	
solvent	E_{ox} (V vs SCE)[a]	ϵ_s	λ_s (eV)[b]	Pe	PeCN
ANI	0.93	7.06[d]	0.58	−0.01	−0.11
NMA	0.81	5.96[d]	0.52	−0.08	−0.18
NEA	0.80	5.87[d]	0.55	−0.09	−0.19
DMA	0.76	4.97[d]	0.45	−0.06	−0.16
DEA	0.72	5.22[e]	0.45	−0.14	−0.24

[a] Oxidation potential (from ref 21), E_{ox}, static dielectric constant, ϵ_s, solvent reorganization energy, λ_s, and ET driving force, ΔG_{ET}. [b] Calculated using eq 6 of ref 50. [c] Calculated using eq 16 of ref 51. [d] From ref 47. [e] From ref 48.

The intramolecular reorganization energy, λ_v, for the ET between aromatic hydrocarbons and anilines has been estimated to increase from about 0.25 to 0.45 eV by going from DEA to ANI.[23] This has been ascribed to the fact that the structural changes experienced by anilines upon ionization depend on the degree of substitution on the N atom. Indeed, the structure around the N atom is planar in the ionized state while it is pyramidal in the neutral form. In the latter case, the extent of pyramidalization decreases with increasing size of the substituents.[52]

The total reorganization energy, $\lambda = \lambda_v + \lambda_s$, for ET in these donating solvents should thus be of the order of 0.7−1 eV. As a consequence, the ET quenching should occur in the normal regime, i.e., the ET time constant should decrease with increasing driving force. Such a trend cannot be really recognized here with τ_{ET}. However, it should not be forgotten that this τ_{ET} value concerns only a subpopulation of the acceptor−donor pairs. Therefore, one should also consider the probability for a donor to perform ultrafast ET. Tables 5 and 6 indicate that n_a, the number of solvent molecules with optimal orientation for ET, exhibits the following solvent dependencies:

(1) For *N*,*N*-dialkylanilines, n_a decreases as the size of the N substituent increases:

$$n_a(\text{DMA}) > n_a(\text{EMA}) > n_a(\text{DEA}) > n_a(\text{DIA})$$

(2) n_a decreases from *N*,*N*-dialkylanilines to *N*-monoalkylanilines and to ANI:

$$n_a(\text{DMA}) > n_a(\text{NMA}) > n_a(\text{ANI}) \text{ and}$$
$$n_a(\text{DEA}) > n_a(\text{NEA}) > n_a(\text{ANI})$$

The first trend is just the inverse of that expected from the driving force. However, it should be noted that the ET driving forces in DMA, EMA, and DEA are quite similar. The above dependence is most certainly due to the steric hindrance.[53] As the size of the alkyl substituent increases, the probability for a donor molecule having an optimal orientation for ET decreases. In other words, the probability for ultrafast ET decreases. The electron-donating properties of these anilines improve upon substitution of the N atom, but this in turn leads to a concomitant increase of their bulkiness.

On the other hand, the second trend shown above can be a manifestation of the effect of driving force. For example, the driving force for the ET quenching of Pe in ANI is so small that the probability for a donor molecule undergoing ultrafast ET, i.e., ET faster than reorientational motion, is negligibly small. Ultrafast ET with ANI might require a stronger electronic coupling than for DMA to counterbalance the smaller driving force. The effect of driving force should even be reinforced by the increase of the reorganization energy by going from DMA and DEA to ANI. Moreover, the parallel increase of the pyramidalization angle around the N atom might also lead to a weakening of the electronic coupling.

As ET proceeds substantially faster than diffusive solvation, the classical Marcus theory should no longer be applied. In the Sumi−Marcus model, which accounts for such situations, ET can take place along fast intramolecular coordinates in time scales faster than diffusive solvation.[54−56] In this case, the effective polarity of the solvent is substantially smaller than that given by the static dielectric constant and therefore both the effective driving force and the reorganization energy are smaller as well. In the extreme case, the effective polarity can be approximated by the square of the refractive index, n^2. In this case, ΔG_{ET} ranges from +0.28 eV for PeCN/DMA to +0.68 eV for Pe/ANI, i.e., ET is clearly endergonic in all solvents. With such ΔG_{ET} values, and even with those listed in Table 7, one would certainly not expect ET to be ultrafast! However, the situation is a bit different here. First, the reactant population is not homogeneous as assumed in the Sumi−Marcus model. In the present case, only a fraction of the reactant population undergoes ET faster than solvation. With Pe, this fraction is very small as shown in Table 5, and might correspond to a subpopulation with highly improbable, statistically insignificant, configurations for which ET is ultrafast. Moreover, as $n_a = np_a$, such configurations would be even rarer if the electron donor was diluted in a nonreactive solvent, i.e., if $n \ll 16$. The subpopulation undergoing ultrafast ET is larger with PeCN, probably because the dipole−dipole interaction favors optimal configurations of the reactants and possibly the solvation as well.

Second, with the systems investigated here, the primary product is an exciplex, i.e., a species without a full charge transfer, and thus the effective driving force for quenching might be larger than that for full ET, due to an additional stabilization energy of the exciplex.[57] Therefore, nonadiabatic theories should be used cautiously.

Early Dynamics of the ET Quenching Product. The fact that the primary quenching product of Pe and PeCN is an exciplex is not really surprising in view of the relatively small polarity of the electron-donating solvents investigated here. Before discussing the exciplex dynamics measured by TCSPC, we will address the early dynamics that looks quite complex, as shown in Figure 4.

From both TG and fluorescence up-conversion measurements, it appears that the formation of the exciplex does not follow a simple precursor−successor kinetic model. First, the rise of the radical anion band is slower than the decay of the excited acceptor band, and second, a rise of the exciplex fluorescence can only be observed on the red side of the exciplex emission spectrum. Moreover, the early fluorescence dynamics in the exciplex region is strongly wavelength dependent. However, Tables 3 and 4 indicate that the average quenching time of PeCN by DMA is 0.42 ps, while the diffusive solvation time is 24.6 ps. This implies that the newly formed exciplex is not stabilized by dipolar solvation, and should thus feel like it is in a nonpolar solvent with a similar refractive index, such as benzene. The PeCN/DMA exciplex spectra in DMA and in benzene ([DMA] = 0.05 M) are compared in Figure 10. By going from benzene to DMA, the emission maximum shifts from 610 to 650 nm, and the quantum yield decreases from 3.3×10^{-2} to 1.1×10^{-4}, while the bandwidth remains almost constant. Similar wavelength shift and decrease of the emission quantum yield are observed with the Pe/DMA exciplex by going from benzene to DMA. Therefore, as solvation occurs, the emission spectrum of the newly formed exciplex in DMA should move to longer wavelengths and its intensity should strongly decrease. Numer-

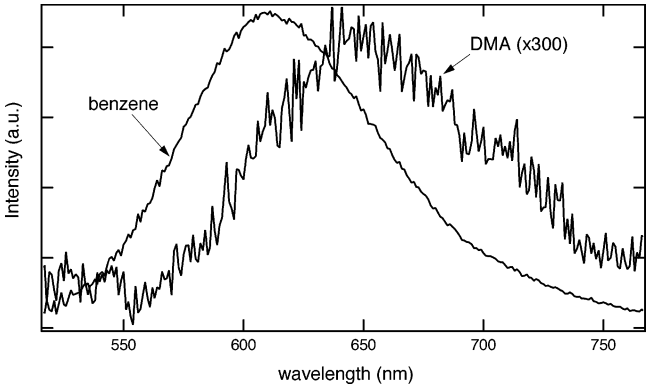

Figure 10. Exciplex fluorescence spectrum of PeCN/DMA in DMA and in benzene ([DMA] = 0.05 M).

ical simulations show that such parallel Stokes shift and intensity decay results in a continuous slowing down of the exciplex fluorescence decay with increasing wavelength. For example, assuming a solvation time of 15 ps, the decay time at 550 and 650 nm amounts to 10 and 23 ps, respectively. The solvation dynamics in DMA has been shown to be biphasic with a 4 ps component, ascribed to the inversion of the amine group, and a 24.6 ps component, assigned to molecular reorientation.[21] The decay time measured in the early exciplex dynamics varies from 7 to 18 ps by going from 600 to 670 nm and therefore corresponds quite well to the time scale of solvation.

Additionally to the pure exciplex emission, local emission from PeCN is still visible up to 700 nm. Therefore, the prompt rise of the fluorescence intensity present at all wavelengths (see Figure 4**)** can be ascribed to this local fluorescence. The initial ultrafast decay component observed at the shortest exciplex wavelengths, $\lambda < 650$ nm, can also be assigned to the local fluorescence. At longer wavelengths, the contribution of the local fluorescence is smaller and a rising component of the exciplex fluorescence can be observed.

The decrease of the exciplex fluorescence yield upon solvation is partially due to a decrease of the radiative rate constant, $k_{r,E}$. In the case of the Pe/DMA and PeCN/DMA exciplexes, $k_{r,E}$ decreases by a factor 8 and 16 respectively by going from benzene to DMA. The following expression shows that the radiative rate constant of an exciplex is related to its charge-transfer (CT) character:[58]

$$f_{CT} \approx 1 - \frac{k_{r,E}}{k_{r,A}}\left(\frac{\nu_A}{\nu_E}\right)^3 \qquad (6)$$

where f_{CT} is the fractional CT character and varies from 0 to 1, ν_A and ν_E are the average fluorescence frequencies of the excited acceptor and of the exciplex, respectively, and $k_{r,A}$ is the radiative rate constant of the excited acceptor. Taking a fluorescence quantum yield of 0.99 for Pe,[59] and 0.96 for PeCN, the radiative rate constants $k_{r,A}$ are 2.2×10^8 s^{-1} and 2.1×10^8 s^{-1} for Pe and PeCN, respectively, while those for the exciplexes can be calculated with the data listed in Table 1. According to eq 6, the fractional CT character of all the exciplexes studied here is larger than 0.98. In principle, this approximate expression should not be used when $f_{CT} > 0.9$. In the latter case, f_{CT} can be determined by using a more complex procedure described in detail in ref 58. According to this more precise method, the CT character of the Pe and PeCN exciplexes in all donating solvents, after solvent relaxation, is essentially unity. Therefore, these exciplexes can be considered as contact ion pairs (CIP). In benzene, f_{CT} is somewhat smaller and amounts to 0.95 and 0.98 for Pe/DMA and PeCN/DMA, respectively.

As a consequence, the CT degree of the exciplexes investigated here, and especially those with Pe, should increase during the first few tens of ps because of the solvation process. Such a variation of the CT character upon solvent relaxation could be at the origin of the different decay and rise times of $^1Pe^*$ and $Pe^{\bullet -}$ TG bands, respectively, and of the narrowing of the $Pe^{\bullet -}$ spectrum shown in Figure 8. A smaller CT character implies a larger contribution of the locally excited state to the exciplex wave function, and thus to a more diffuse transient spectrum.[60] The narrowing of the TG band is accompanied by an increase of the maximum intensity. Therefore, if the narrowing occurs in a slightly slower time scale than ET quenching, the kinetics of product formation, when measured at the band maximum, will appear to be slower than the decay dynamics of the reactant population. The narrowing and the delayed rise take place in the 10−20 ps time scale, in agreement with the time scale of solvent relaxation.

The early dynamics of the ET quenching product can thus be summarized as follows:

$$A^*{\cdot}D \xrightarrow{ET} (A^{\delta_1-}{\cdot}D^{\delta_1+}) \xrightarrow{solv} (A^{\delta_2-}{\cdot}D^{\delta_2+})$$

The final ET quenching product is an exciplex with essentially full CT, i.e., a CIP. Its fluorescence yield is therefore extremely small and its TG spectrum very similar to that of the ions. However, because it is formed in a time scale shorter than solvation, the primary product is an exciplex with a smaller CT character, hence with a larger emission yield and a broader TG spectrum.

Slow Dynamics of the ET Quenching Product. The TG spectra, measured at time delays longer than a few tens of a picosecond, are very similar to those of $Pe^{\bullet -}$ and $PeCN^{\bullet -}$ measured in polar solvents, as expected for CIPs. In highly polar solvents, the major deactivation pathways of exciplexes and CIPs are the charge recombination to the neutral ground state and the dissociation to a loose ion pair and/or to free ions.[61−63] In lower polarity solvents, intersystem crossing (ISC) to the triplet excited state of one of the neutral reactants can also be operative. In the absence of a strong spin−orbit coupling, due for example to the presence of a heavy atom[64] or to a specific geometry of the exciplex,[65] the ISC rate constant is small, of the order of $(1-5) \times 10^6$ s^{-1}.[62,66−68] Therefore, this deactivation pathway should not be significant for the exciplexes investigated here, especially those with PeCN. Exciplexes with primary and secondary amines are also known to decay by proton transfer.[69] For exciplexes with a polyaromatic hydrocarbon as acceptor, this process has only been reported in nonpolar solvents, where the ion pair state is less stable than the neutral proton-transfer product.[62,70] No evidence of proton transfer, new transient band or permanent photoproduct, was found with Pe and PeCN in ANI, NMA, and NEA. This is in total agreement with the studies of Mataga and co-workers showing that proton transfer after ET quenching of pyrene by ANI occurs only in nonpolar solvents, like toluene and cyclohexane, but not in pure ANI.[62,70]

Finally, the dissociation of an exciplex or a CIP to a loose ion pair or to free ions is a diffusive process and is thus strongly viscosity dependent.[61] As Tables 1 and 4 do not indicate any correlation between the exciplex fluorescence lifetime and solvent viscosity, one can presume that the exciplex dissociation is not significant in these relatively weakly polar solvents. Therefore, the main deactivation pathways of the CIPs investigated here are most probably CR.

The driving force for the charge recombination of these CIPs, ΔG_{CR}, can be calculated as $\Delta G_{CR} = -E(S_1) - \Delta G_{ET}$, where $E(S_1)$ is the S_1 energy of the acceptor and amounts to 2.8 and

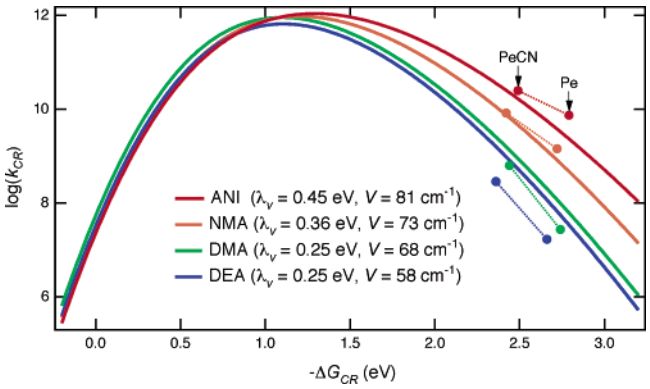

Figure 11. Rate constants of CR of the exciplexes formed upon quenching of Pe and PeCN in ANI, NMA, DMA, and DEA (filled circles) as a function of the driving force and free energy dependencies for CR of ion pairs formed upon quenching of aromatic hydrocarbons by ANI, NMA, DMA, and DEA in acetonitrile (continuous lines, from ref 23).

2.6 eV for Pe and PeCN, respectively. Using the ΔG_{ET} values listed in Table 7, it appears that the driving force for CR ranges from −2.79 to −2.66 eV for Pe and from −2.49 to −2.36 for PeCN. Therefore, CR should take place in the inverted region and an increase of the exciplex lifetime with increasing CR driving force should be expected. Table 1 shows that this is clearly not the case and that there is no apparent correlation between τ_E and ΔG_{CR}. In a recent investigation of the CR dynamics of ion pairs formed upon ET quenching of several aromatic hydrocarbons by different types of electron donors, among them aniline derivatives, in acetonitrile, an apparently poor correlation of the CR rate constants with the driving force was found.[23] However, when sorted according to the electron donors, the k_{CR} data were found to exhibit distinct free energy dependencies. The calculated free energy dependencies obtained by fitting the semiclassical expression for nonadiabatic ET to the CR rate constants measured with ANI, NMA, DMA, and DEA are shown in Figure 11. These curves were calculated with the same solvent reorganization energy, $\lambda_s = 0.9$ eV, but with different electronic coupling constant, V, and/or, intramolecular reorganization energy, λ_v. The decrease of the coupling constant with increasing size of the N atom substituents was ascribed to the effect of charge dilution. Because of the extended charge delocalization in the *N*,*N*-dialkylanilines, the wave functions involved in the CR are more diffuse and thus the electronic-coupling matrix element V is smaller.[39] As discussed above, the increase of λ_v by going from DEA to ANI can be related to the pyramidalization angle around the N atom of the neutral anilines.

The full circles in Figure 11 are the CR rate constants of the CIPs investigated here, with $k_{CR} = \tau_E^{-1}$. This figure shows that these apparently strongly scattered data match very well the free energy dependencies found in the previous study in acetonitrile.[23] From this figure, it appears that the donor dependence of k_{CR} at a fixed driving force is more pronounced with the CIPs investigated here. A better matching of the points with the curves could be obtained by shifting these curves upward and to the right. This would correspond to an increase of the electronic coupling matrix element V and to a decrease of the solvent reorganization energy. The latter point is of course reasonable if one considers that the solvent reorganization energy in acetonitrile was estimated to amount to 0.9 eV, while that in the anilines is substantially smaller. A larger electronic coupling can also be justified by the fact that the CIPs exhibit fluorescence while the ion pairs investigated in the previous study were totally nonfluorescent.[23]

However, the comparison presented in Figure 11 is enough to show that the shorter fluorescence lifetimes measured with PeCN can be totally accounted for by the smaller driving force of CR and its strong solvent dependence can be explained in terms of different V and λ_v values.

Concluding Remarks

We have presented here a detailed study of the electron-transfer quenching dynamics of Pe and PeCN in various electron-donating solvents as well as the dynamics of product formation and decay.

The solvent dependence of the ET quenching can be qualitatively well accounted for when the dynamics is analyzed with the orientational model. This model is of course crude but takes into account the statistical nature of the orientation of the donor molecules around the electron acceptor. According to this analysis, the ET time constant for optimal orientation of the reactants does not change very much from one solvent to another. However, the probability for a donor molecule to be in an adequate orientation for ultrafast ET changes significantly from one acceptor/donor system to another. This probability seems mainly influenced by dipole−dipole interactions, by steric effects, and by the driving force: the larger the driving force and the smaller the steric hindrance, the higher the probability for a donor molecule to undergo ultrafast ET. In donating solvents, the number of donor molecules is so large that even statistically weakly significant events can be observed. This must be the case, for example, for the ultrafast ET between Pe and the donating solvents used here.

The donating solvents also offer the opportunity to observe the early dynamics of exciplexes. With diluted donor solutions, the quenching is much slower and therefore the dipolar solvation dynamics of the exciplex cannot be investigated. The present study gives some indication that the final charge transfer character of the ET quenching product is only achieved after solvent relaxation. More detailed measurements are still needed for obtaining a more quantitative picture of this process.

Finally, this investigation has also shown that once the quenching is over, the electron-donating solvents behave essentially as inert solvents. Indeed, the donor dependence of the charge recombination dynamics measured here is very similar to that found with geminate ion pairs in acetonitrile.

Acknowledgment. This work was supported by the Fonds National Suisse de la Recherche Scientifique through project No. 200020-100014.

References and Notes

(1) Morandeira, A.; Fürstenberg, A.; Gumy, J.-C.; Vauthey, E. *J. Phys. Chem. A* **2003**, *107*, 5375.
(2) Kobayashi, T.; Tagaki, Y.; Kandori, H.; Kemnitz, K.; Yoshihara, K. *Chem. Phys. Lett.* **1991**, *180*, 416.
(3) Rubstov, I. V.; Shirota, H.; Yoshihara, K. *J. Phys. Chem. A* **1999**, *103*, 1801.
(4) Yoshihara, K.; Tominaga, K.; Nagasawa, Y. *Bull. Chem. Soc. Jpn.* **1995**, *68*, 696.
(5) Yoshihara, K. Ultrafast Intermolecular Electron Transfer in Solution. In *Electron Transfer*: *From Isolated Molecules to Biomolecules*; Jortner, J., Bixon, M., Eds.; John Wiley: New York, 1999; Vol. 107, p 371.
(6) Engleitner, S.; Seel, M.; Zinth, W. *J. Phys. Chem. A* **1999**, *103*, 3013.
(7) Seel, M.; Engleitner, S.; Zinth, W. *Chem. Phys. Lett.* **1997**, *275*, 363.
(8) Wolfseder, B.; Seidner, L.; Domcke, W.; Stock, G.; Seel, M.; Engleitner, S.; Zinth, W. *Chem. Phys.* **1998**, *233*, 323.
(9) Iwai, S.; Murata, S.; Tachiya, M. *J. Chem. Phys.* **1998**, *109*, 5963.
(10) Iwai, S.; Murata, S.; Katoh, R.; Tachiya, M.; Kikuchi, K.; Takahashi, Y. *J. Chem. Phys.* **2000**, *112*, 7111.

(11) Castner, E. W., Jr.; Kennedy, D.; Cave, R. J. *J. Phys. Chem. A* **2000**, *104*, 2869.
(12) Xu, Q.-H.; Scholes, G. D.; Yang, M.; Fleming, G. R. *J. Phys. Chem. A* **1999**, *103*, 10348.
(13) Rehm, D.; Weller, A. *Isr. J. Chem.* **1970**, *8*, 259.
(14) Nishikawa, S.; Asahi, T.; Okada, T.; Mataga, N.; Kakitani, T. *Chem. Phys. Lett.* **1991**, *185*, 237.
(15) Murata, S.; Nishimura, M.; Matsuzaki, S. Y.; Tachiya, M. *Chem. Phys. Lett.* **1994**, *200*, 219.
(16) Jacques, P.; Allonas, X. *Chem. Phys. Lett.* **1995**, *233*, 533.
(17) Scully, A. D.; Takeda, T.; Okamoto, M.; Hirayama, S. *Chem. Phys. Lett.* **1994**, *228*, 32.
(18) Swallen, S. F.; Weidemaier, K.; Tavernier, H. L.; Fayer, M. D. *J. Phys. Chem.* **1996**, *100*, 8106.
(19) Gladkikh, V. S.; Burshtein, A. I.; Tavernier, H. L.; Fayer, M. D. *J. Phys. Chem. A* **2002**, *106*, 6982.
(20) Scherer, P. O. J. *J. Phys. Chem. A* **2000**, *104*, 6301.
(21) Shirota, H.; Pal, H.; Tominaga, K.; Yoshihara, K. *J. Phys. Chem. A* **1998**, *102*, 3089.
(22) Kandori, H.; Kemnitz, K.; Yoshihara, K. *J. Phys. Chem.* **1992**, *96*, 8042.
(23) Vauthey, E. *J. Phys. Chem. A* **2001**, *105*, 340.
(24) Buu-Hoï, N. P.; Long, C. T. *Recl. Trav. Chim. Pays-Bas* **1956**, *75*.
(25) Armagero, W. L. F.; Chai, C. L. L. *Purification of Laboratory Chemicals*; Elsevier: Amsterdam, The Netherlands, 2003.
(26) Riddick, J. A.; Bunger, W. B. *Organic Solvents*; J. Wiley: New York, 1970.
(27) Leonhart, H.; Weller, A. *Ber. Bunsen-Ges. Phys. Chem.* **1963**, *67*, 791.
(28) Knibbe, H.; Rehm, D.; Weller, A. *Ber. Bunsen-Ges.* **1968**, *72*, 257.
(29) Mataga, N.; Kiyoshi, E. *Bull. Chem. Soc. Jpn.* **1967**, *40*, 1355.
(30) Pigliucci, A.; Vauthey, E. *Chimia* **2003**, *57*, 200.
(31) Pagès, S.; Lang, B.; Vauthey, E. *J. Phys. Chem. A* **2004**, *108*, 549.
(32) Hochstrasser, R. M.; Nyi, C. *J. Chem. Phys.* **1980**, *72*, 2591.
(33) Ong, K. K.; Jensen, J. O.; Hameka, H. F. *J. Mol. Struct.* (*THEOCHEM*) **1999**, *459*, 131.
(34) Edholm, O.; Blomberg, C. *Chem. Phys.* **1999**, *252*, 221.
(35) Fayer, M. D. *Annu. Rev. Phys. Chem.* **1982**, *33*, 63.
(36) Fourkas, J. T.; Fayer, M. D. *Acc. Chem. Res.* **1992**, *25*, 227.
(37) Högemann, C.; Pauchard, M.; Vauthey, E. *Rev. Sci. Instrum.* **1996**, *67*, 3449.
(38) Högemann, C.; Vauthey, E. *Isr. J. Chem.* **1998**, *38*, 181.
(39) Vauthey, E. *J. Phys. Chem.* **2000**, *104*, 1804.
(40) Shida, T. *Electronic Absorption Spectra of Radical Ions*; Physical Sciences Data, No. 34; Elsevier: Amsterdam, The Netherlands, 1988.
(41) Muller, P.-A. Ph.D. Thesis, University of Fribourg, 2001.
(42) Shirota, H.; Pal, H.; Tominaga, K.; Yoshihara, K. *Chem. Phys.* **1998**, *236*, 355.
(43) Smith, N. A.; Lin, S.; Meech, S. R.; Yoshihara, K. *J. Phys. Chem.* **1997**, *101*, 3641.
(44) Garg, S. K.; Smyth, C. P. *J. Chem. Phys.* **1967**, *46*, 373.
(45) Smith, N. A.; Lin, S.; Meech, S. R.; Shirota, H.; Yoshihara, K. *J. Chem. Phys. A* **1997**, *101*, 9578.
(46) Edward, J. T. *J. Chem. Educ.* **1970**, *4*, 261.
(47) *Handbook of Chemistry and Physics*, 82nd ed.; Lide, D. R., Ed.; CRC Press: Boca Raton, FL, 2001.
(48) Price, A. H. *J. Phys. Chem.* **1958**, *62*, 773.
(49) Spernol, A.; Wirtz, K. *Z. Naturforsch.* **1953**, *8a*, 522.
(50) Marcus, R. A.; Sutin, N. *Biochim. Biophys. Acta* **1985**, *811*, 265.
(51) Weller, A. *Z. Phys. Chem. N. F.* **1982**, *133*, 93.
(52) Bock, H.; Göbel, I.; Havlas, Z.; Liedle, S.; Oberhammer, H. *Angew. Chem.* **1991**, *103*, 193.
(53) Hubig, S. M.; Rathore, R.; Kochi, J. K. *J. Am. Chem. Soc.* **1999**, *121*, 617.
(54) Sumi, H.; Marcus, R. A. *J. Chem. Phys.* **1986**, *84*, 4894.
(55) Sumi, H.; Marcus, R. A. *J. Chem. Phys.* **1986**, *84*, 4272.
(56) Sumi, H. *J. Mol. Liquids* **1985**, *65/66*, 65.
(57) Weller, A. In *The Exciplex*; Gordon, M., Ware, W. R., Eds.; Academic Press: New York, 1975; p 23.
(58) Gould, I. R.; Young, R. H.; Mueller, L. J.; Albrecht, A. C.; Farid, S. *J. Am. Chem. Soc.* **1994**, *116*, 8188.
(59) Dawson, W. R.; Windsor, M. W. *J. Phys. Chem.* **1968**, *72*, 3251.
(60) Ottolenghi, M. *Acc. Chem. Res.* **1973**, *6*, 153.
(61) Weller, A. *Pure Appl. Chem.* **1982**, *54*, 1885.
(62) Mataga, N.; Miyasaka, H. *Adv. Chem. Phys.* **1999**, *107*, 431.
(63) Vauthey, E.; Högemann, C.; Allonas, X. *J. Phys. Chem. A* **1998**, *102*, 7362.
(64) Hamai, S. *Bull. Chem. Soc. Jpn.* **1984**, *57*, 2700.
(65) Okada, T.; Karaki, I.; Matsuzawa, E.; Mataga, N.; Sakata, Y.; Misumi, S. *J. Phys. Chem.* **1981**, *85*, 3957.
(66) Kuzmin, M. G. *J. Photochem. Photobiol. A* **1996**, *102*, 51.
(67) Gould, I. R.; Boiani, J. A.; Gaillard, E. B.; Goodman, J. L.; Farid, S. *J. Phys. Chem. A* **2003**, *107*, 3515.
(68) Watkins, A. R. *J. Phys. Chem.* **1979**, *83*, 1892.
(69) Yang, N. C.; Libman, J. *J. Am. Chem. Soc.* **1973**, *95*, 5783.
(70) Okada, T.; Karaki, I.; Mataga, N. *J. Am. Chem. Soc.* **1982**, *104*, 7191.